# California foreshock sequences suggest aseismic triggering process

Xiaowei Chen,[1] Peter M. Shearer,[1]

---

X. Chen, Scripps Institution of Oceanography, University of California, San Diego, La Jolla, California, USA. (xic002@ucsd.edu)

P. M. Shearer, Scripps Institution of Oceanography, University of California, San Diego, La Jolla, California, USA.

[1] Scripps Institution of Oceanography,
University of California, San Diego, La
Jolla, California, USA.

Foreshocks are one of the few well-documented precursors to large earthquakes; therefore, understanding their nature is very important for earthquake prediction and hazard mitigation. However, the triggering role of foreshocks is not yet clear. It is possible that foreshocks are a self-triggering cascade of events that simply happen to trigger an unusually large aftershock; alternatively, foreshocks might originate from an external aseismic process that ultimately triggers the mainshock. In the former case, the foreshocks will have limited utility for forecasting. The latter case has been observed for several individual large earthquakes, however, it remains unclear how common it is, and how to distinguish foreshock sequences from other seismicity clusters that do not lead to large earthquakes. Here, we analyze foreshocks of three $\mathrm{M} > 7$ mainshocks in southern California. These foreshock sequences appear similar to earthquake swarms, in that they do not start with their largest events and they exhibit spatial migration of seismicity. Analysis of source spectra shows that all three foreshock sequences feature lower average stress drops and depletion of high-frequency energy compared with the aftershocks of their corresponding mainshocks. Using a longer-term stress drop catalog, we find that the average stress drop of the Landers and Hector Mine foreshock sequences are comparable to nearby swarms. Our observations suggest that these foreshock sequences are manifestations of aseismic transients occurring close to the mainshock hypocenters, possibly related to localized fault zone complexity, which have promoted the occurrence of both the foreshocks and the eventual mainshocks.

## 1. Introduction

Foreshock sequences are the most obvious precursor to large earthquakes; therefore, understanding their origin and relation to mainshocks is of great importance for earthquake prediction and hazard mitigation. Previous studies of immediate foreshocks in California suggest that these events may be part of a mainshock rupture nucleation process, because estimated Coulomb stress changes from foreshocks are too small to produce stress triggering and observed foreshock areas scale with mainshock magnitude, consistent with nucleation rather than earthquake-to-earthquake triggering [*Dodge et al.*, 1996]. For the 1999 Izmit earthquake, accelerating repeating events originating from near the mainshock hypocenter suggest an extended nucleation process [*Bouchon et al.*, 2012]. For the 2011 Tohoku earthquake, a quasi-static slip transient was observed from foreshock sequences with repeating earthquakes, but its properties differ from expectation from the pre-slip nucleation model [*Ando and Imanishi*, 2012; *Kato et al.*, 2012]. Despite the observations for several individual earthquakes, however, some questions remain unclear, such as: (1) does the aseismic triggering process generalize to other mainshocks?, and (2) are there any physical properties that distinguish foreshocks from other sequences? Here, we use a recently compiled high-resolution earthquake catalog [*Hauksson et al.*, 2012], and apply a source spectral analysis method [*Shearer et al.*, 2006] to study foreshock sequences in southern California and compare their properties to other nearby earthquakes.

## 2. Spatial-temporal pattern

There are three M > 7 earthquakes in the catalog since 1981: 1992 Mw 7.3 Landers, 1999 Mw 7.1 Hector Mine, and 2010 Mw 7.2 El Mayor-Cucapah (Figure 1). All of them are dominated by strike-slip faulting (a normal-faulting sub-event exists for the El Mayor-Cucapah earthquake), located along secondary faults adjacent to the main North America-Pacific plate boundary [*Hauksson et al.*, 2012]. The Landers earthquake is preceded by 27 cataloged foreshocks within 7 hr and 1.5 km. The Hector Mine earthquake has 18 cataloged foreshocks within 24 hr and 0.5 km. The El Mayor-Cucapah earthquake is preceded by an extended foreshock sequence, which is separated into two distinct time periods: the first occurred on March 21, and the second occurred on April 3, 30 hr before the mainshock; the foreshocks extend up to 6 km from the mainshock. The foreshock magnitudes range from 1.2 to 4.4 for all three cases with no clear “mainshock” within the foreshock sequences (Figure 2 and Figure S8).

To obtain greater relative location accuracy between the mainshock hypocenters and their foreshock sequences, we first apply a custom relocation method (see Methods). We then use a weighted-L1-norm approach [*Chen and Shearer*, 2011] to model the spatial migration of the foreshock sequences (Figure S1). The Landers foreshock sequence is separated into two periods: the first starts at -7 hr, lasts about 2 hours, and spreads across the entire foreshock region; the second starts at -2.5 hr, and migrates northward toward the mainshock at about 0.6 km/hr. The El Mayor-Cucapah sequence exhibits similar behavior: the first part quickly spans almost the entire foreshock region, and the second part migrates northward at about 0.5 km/hr. The Hector Mine foreshock sequence also migrates northward, but at a much lower velocity of about 0.03 km/hr, similar to swarms thought to be triggered by fluid flow [*Chen et al.*, 2012]. Modeling this sequence with fluid diffusive migration yields a slightly lower misfit compared to the linear migration model; the best-fitting diffusion coefficient is 0.2 $\mathrm{m}^2/\mathrm{s}$, consistent with swarms in the Salton Trough [*Chen and Shearer*, 2011].

All of the foreshock sequences appear associated with fault zone complexity (Figure 1). The Landers foreshocks are located at a jog between two fault segments [*Dodge et al.*, 1996]. The Hector Mine foreshocks are located at a branch of the main fault trace and the foreshocks themselves define a small branch (Figure S1). The El Mayor-Cucapah foreshocks outline a nearly north-south striking fault plane, whereas the main fault trace strikes N50°W [*Hauksson et al.*, 2011]. The El Mayor-Cucapah mainshock initiated on an extensional jog at depth, with a similar strike but different dip as a M 4.4 foreshock [*Hauksson et al.*, 2011; *Wei et al.*, 2012]. In all three cases, the final stage of migration started at a region of local complexity in the fault zone (Figure S1).

## 3. Source spectra

For each mainshock sequence, we obtain event source spectra from an iterative deconvolution approach. We then correct individual source spectral using an empirical Green's function method [*Shearer et al.*, 2006], fit to a Brune-type source model $u(f) = \frac{\Omega_0}{1+(f/f_c)^2}$ to obtain corner frequency ($f_c$) [*Brune*, 1969], and compute stress drop from the *Madariaga* [1976] relation $\Delta\sigma = \frac{f_c^3 M_0}{(0.42\beta)^3}$. This formula assumes the rupture velocity $v_r = 0.9\beta$, where $\beta$ is the shear wave velocity. For convenience some previous stress drop studies have assumed a fixed rupture velocity for all events (e.g., *Shearer et al.*, [2006]), but as shown by [*Allmann and Shearer*, 2007] for the Parkfield region, this can lead to an artificial increase in computed stress drop with depth even if stress drop itself is constant, because rupture velocity likely increases with depth in proportion to the shear-wave velocity. To account for these depth variations, we compute stress drops using rupture velocities inferred from a depth-dependent shear velocity model for southern California (see Figure S5) [*Shearer et al.*, 2005]. The estimated stress drops follow a log-normal distribution and do not depend on event magnitude, indicating self-similar behavior. We compare the median stress drops for foreshocks and aftershocks within 3.3 km (6.6 km for El Mayor-Cucapah) and 5 days from each mainshock, and find that the median foreshock stress drops are substantially lower than that of the corresponding aftershocks (Figure 3). Aftershock stress drops in this area stay at a relatively high level for a much longer time period (see Figure S6 and S7 for aftershocks in 20 days and 100 days, respectively).

The *Shearer et al.* [2006] study of southern California stress drops indicated substantial spatial variations in median stress drops, generally over larger distances than the size of the boxes we use to sample the aftershocks, but sometimes over shorter scales. Thus, the question arises as to whether our observed foreshock stress drops are lower because the foreshocks are fundamentally different than the aftershocks or whether they happen to sample a region that is prone to lower stress drops than that sampled by the aftershocks. To control for the latter possibility, ideally the foreshocks and aftershocks would sample exactly the same area. Unfortunately that is not possible in our case because the foreshocks are in a very compact region that is not sampled by immediate aftershocks. We have, however, attempted to use aftershocks as close as possible to the foreshocks, while still retaining enough aftershocks to obtain reliable median stress drops, given the scatter in individual events stress drops. There is also the possibility that our corrections for depth dependent rupture velocity are inaccurate and differences in foreshock versus aftershock depth could account for our result. This explanation doesn't work for the Hector Mine and El Mayor-Cucapah sequences, in which the foreshocks and aftershocks span similar depth ranges (see Figure S4). However, it could apply to the Landers sequence, where the foreshocks are confined within a narrow shallow depth range around 2 km, while most aftershocks are much deeper (Figure S4). If we remove an empirical depth-dependent stress drop trend for the Landers sequence, the foreshock stress drops increase to a similar level as the aftershocks. However, this adjustment would exceed the correction expected simply from the shear-velocity increase with depth, which has already been applied.

It is also possible that attenuation changes after a large earthquake could affect the EGF-corrected source spectra and the stress-drop estimates. To test for this possibility, we compute separate EGFs for the foreshocks and aftershocks, and estimate the change in t* from their spectral ratio [*Shearer*, 2009]. The increase in t* suggests increased attenuation after the mainshocks (Figure S2). However, due to the limited number of available foreshock source spectra, this result is not stable with respect to the choice of different magnitude bins and thus these attenuation changes are not reliably resolved. Nonetheless, it seems unlikely that our result (lower stress drop estimates for foreshocks) is an artifact of attenuation changes, because this would require attenuation to decrease as a result of the mainshock, opposite to what previous studies have found. For example, increased attenuation was observed following the 1989 Loma Prieta and 2004 Parkfield earthquakes, possibly due to increased pore creation and fault zone damage after the mainshock [*Chun et al.*, 2004; *Allmann and Shearer*, 2007].

The absolute level of our estimated stress drops depends upon a number of modeling assumptions, but the relative differences indicate variations in the source spectra that are robust with respect to our modeling choices. To confirm these differences, we directly compare the stacked foreshock and aftershock spectra, and find that foreshock spectra are consistently depleted in high-frequency energy, and exhibit a faster fall-off rate than the aftershock spectra. To validate our deconvolution process, we also examine the P-wave spectra at individual stations, and find the original displacement spectra exhibit similar behavior (see example in Figure S3). These results indicate that the observed differences in median stress drop reflect real differences in the earthquake source spectra. This is our most robust result, because it does not depend upon an assumed rupture model or source location. The foreshock records are depleted in high-frequency energy compared to nearby aftershocks.

To better understand the short-term stress-drop variations occurring at the time of the mainshock, it is important to examine the longer-term stress-drop behavior in the same region. Using the stress-drop catalog for southern California from 1989 to 2002 [*Shearer et al.*, 2006], we examined the complete stress-drop history within the vicinity of the Landers and Hector Mine mainshocks (Figure 4 and 5). It should be noted that individual stress drop measurements are different from the values in Figure 3, where different station terms and empirical Green's functions are used. We select events within 15 km from the fault zone of the Landers and Hector Mine earthquakes, and compare median stress drop for different time periods (see Figure 4 and 5): (a) before the Joshua Tree earthquake (about two months before the Landers earthquake), (b) between the Joshua Tree and

Landers earthquakes, (c) between the Landers and Hector Mine earthquakes, (d) after the Hector Mine earthquake. For each time period, we divide events in several bins according to occurrence time, and find the median stress drop for each bin.

Several interesting features are noted from Figures 4 and 5. In both cases, the long-term average stress drop is relatively stable, although a slow increase trend of stress drop after large mainshocks within the Landers fault zone is observed, possibly indicating long-term fault zone recovery [*Li et al.*, 1998]. Background seismicity prior to Joshua Tree earthquake is mostly located surrounding the epicenter of the Joshua Tree earthquake (Figure 4a). Immediately before the Landers earthquake, foreshock stress drops are anomalously low. Stress drops returned to the background level after the Landers earthquake. Within the Hector Mine mainshock epicenter zone, seismicity increased after Landers earthquake and clustered near the eventual Hector Mine mainshock (Figure 5c). The overall average stress drop is lower compared with the Landers region, however, after the Hector Mine mainshock, the stress drop slightly increased. The foreshock stress drop is similar to background level within the Hector Mine region. For comparison, we also plot the average stress drops and locations for "burst-like" clusters in this region from *Vidale and Shearer* [2006]. Among them, bursts 49 and 64 are possibly secondary triggered aftershock sequences after the Landers and Hector Mine mainshocks. Burst 52 is an extended swarm-like sequence that migrated at very low speed (about 0.001 km/hr), and was most likely triggered by a fluid signal (D=0.03 $m^2/s$). Burst 31 is a small swarm that does not show spatial migration. All but burst 31 exhibit lower than average stress drops, however, bursts 52 and 64 are located to the north of Hector Mine rupture zone.

## 4. Discussion

Quasi-static slip signals prior to rapid dynamic rupture have been observed from numerical modeling and laboratory observations [*Ohnaka and Shen*, 1999; *Lapusta and Rice*, 2003]. Emergent onsets in seismic waveforms and immediate foreshock sequences have been interpreted to represent a slow nucleation process [*Dodge et al.*, 1996; *Ellsworth and Beroza*, 1995]. However, the observed spatial-temporal evolution patterns for the foreshocks studied here differ from a nucleation-related pre-slip model. There is no temporal acceleration of foreshock occurrence, and the three similar sized mainshocks have very different foreshock areas and durations (Figure 2 and 3), suggesting no simple scaling relationship with mainshock magnitude [*Abercrombie and Mori*, 1996]. Rather, the spatial pattern resembles features of earthquake swarms in the vicinity, where an external aseismic transient is likely involved.

For the Landers and El Mayor-Cucapah earthquakes, observations of smaller sub-events [*Wei et al.*, 2012; *Abercrombie and Mori*, 1994] indicate that the direct mainshock nucleation may start after the last observed foreshocks. It is interesting to note the association between fault zone complexity [*Jones*, 1984] and the foreshock migration pattern. Both numerical modeling and laboratory experiments have found that fault zone complexity is critical in the generation of smaller events [*Ohnaka and Shen*, 1999; *Lapusta and Rice*, 2003; *Rice and Ben-Zion*, 1996]. For a constant shear loading on a rough fault, the shear stress accumulates non-uniformly along the fault zone with concentration at stronger positions. The failure starts at weaker positions and grows at 0.3 to 4 km/hr [*Ohnaka and Shen*, 1999], consistent with our observed foreshock migration rate. In this scenario, stress loading from the external transient event accumulates within the localized area, in which abrupt failure events are promoted. Due to strong heterogeneity, the critical pore creation slip distance is small [*Yamashita*, 1999], and swarm-like behavior is generated. The transient event then causes stress loading at the mainshock hypocenter, which may trigger the eventual mainshocks. The origin and nature of the hypothesized transient event is unknown, but either slow slip or fluid flow could lead to reduced fault strength and lowered differential stress [*Chen and Shearer*, 2011; *Allmann et al.*, 2010], which could account for the smaller stress drops seen for the foreshocks. Not all large earthquakes are preceded by observable foreshock sequences and not all swarms lead to large earthquakes. But our results suggest that many foreshock sequences, like swarms, may reflect an underlying aseismic triggering process. For the Eastern California Shear Zone, small seismicity bursts are less frequent than in other parts of southern California [*Chen et al.*, 2012]; therefore, at least in this region, burst occurrence may be a useful contributor to short-term earthquake probability estimates. Between 1989 and 2002, only four seismic "bursts" occurred within this region that meet the criteria in [*Vidale and Shearer*, 2006], and two are swarms without clear mainshocks. The 2 foreshock sequences are also swarm-like "bursts" that occurred within fault zone complexity zone.

**Acknowledgments.** We thank Yuri Fialko for helpful discussion and surface fault trace data. We also thank the SCSN network and SCEC data center for providing earthquake catalog and waveform data for analysis. We also thank editor Andrew Newman and two anonymous reviewers for their constructive comments.

## References

Abercrombie, R., and J. Mori (1994), Local observations of the onset of a large earthquake - 28 June 1992 Landers, California, *Bulletin of the Seismological Society of America*, *84*(3), 725–734.

Abercrombie, R. E., and J. Mori (1996), Occurrence patterns of foreshocks to large earthquakes in the Western United States, *Nature*, *381*(6580), 303–307.

Allmann, B. P., and P. M. Shearer (2007), Spatial and temporal stress drop variations in small earthquakes near Parkfield, California, *Journal of Geophysical Research-Solid Earth*, *112*(B4), 17.

Allmann, B. P., A. Goertz, and S. Wiemer (2010), Stress drop variations of induces earthquakes at the Basel geothermal site, *Geophysical Research Letters*.

Ando, R., and K. Imanishi (2012), Possibility of M-w 9.0 mainshock triggered by diffusional propagation of after-slip from M-w 7.3 foreshock, *Earth Planets and Space*, *63*(7), 767–771.

Bouchon, M., H. Karabulut, M. Aktar, S. Ozalaybey, J. Schmittbuhl, and M. P. Bouin (2012), Extended nucleation of the 1999 M-w 7.6 Izmit earthquake, *Science*, *331*(6019), 877–880.

Brune, J. N. (1969), Tectonic stress and the spectra of seismic shear waves from earthquakes, *J. Geophys. Res.*, *75*.

Chen, X., and P. M. Shearer (2011), Comprehensive analysis of earthquake source spectra and swarms in the Salton Trough, California, *J. Geophys. Res.*, *116*(B09309).

Chen, X., P. M. Shearer, F. Walter, and H. A. Fricker (2011), Seventeen Antarctic seismic events detected by global surface waves and a possible link to calving events from satellite images, *J. Geophys. Res.*, *116*(B06311).

Chen, X., P. M. Shearer, and R. Abercrombie (2012), Spatial migration of earthquakes within seismic clusters in southern California: Evidence for fluid diffusion, *J. Geophys. Res.*, *117*(B04301).

Chun, K.-Y., G. A. Henderson, and J. Liu (2004), Temporal changes in p wave attenuation in the Loma Prieta rupture zone, *J. Geophys. Res.*, *109*(B2), B02,317.

Dodge, D. A., G. C. Beroza, and W. L. Ellsworth (1996), Detailed observations of California foreshock sequences: Implications for the earthquake initiation process, *Journal of Geophysical Research-Solid Earth*, *101*(B10), 22,371–22,392.

Ellsworth, W. L., and G. C. Beroza (1995), Seismic evidence for an earthquake nucleation phase, *Science*, *268*(5212), 851–855.

Hauksson, E., J. Stock, K. Hutton, W. Z. Yang, J. A. Vidal-Villegas, and H. Kanamori (2011), The 2010 m (w) 7.2 el mayor-cucapah earthquake sequence, Baja California, Mexico and southernmost California, USA: Active seismotectonics along the Mexican Pacific margin, *Pure and Applied Geophysics*, *168*(8-9), 1255–1277.

Hauksson, E., W. Yang, and P. M. Shearer (2012), Waveform relocated earthquake catalog for southern California (1981 to June 2011), *Bulletin of the Seismological Society of America*, *102*(5), 2239–2244.

Jones, L. M. (1984), Foreshocks (1966-1980) in the San-Andreas system, California, *Bulletin of the Seismological Society of America*, *74*(4), 1361–1380.

Kato, A., K. Obara, T. Igarashi, H. Tsuruoka, S. Nakagawa, and N. Hirata (2012), Propagation of slow slip leading up to the 2011 M-w 9.0 Tohoku-Oki earthquake, *Science*, *335*(6069), 705–708.

Lapusta, N., and J. R. Rice (2003), Nucleation and early seismic propagation of small and large events in a crustal earthquake model, *J. Geophys. Res.*, *108*(B4), 2205.

Li, Y. G., J. E. Vidale, K. Aki, F. Xu, and T. Burdette (1998), Evidence of shallow fault zone strengthening after the 1992 M7.5 Landers, California, earthquake, *Science*, *279*(5348), 217–219.

Lin, G. Q., P. M. Shearer, and E. Hauksson (2007), Applying a three-dimensional velocity model, waveform cross correlation, and cluster analysis to locate southern California seismicity from 1981 to 2005, *Journal of Geophysical Research-Solid Earth*, *112*(B12), 14.

Madariaga, R. (1976), Dynamics of an expanding circular fault, *Bull. Seismol. Soc. Am.*, *66*, 639–666.

Ohnaka, M., and L. Shen (1999), Scaling of the shear rupture process from nucleation to dynamic propagation: Implications of geometric irregularity of the rupturing surfaces, *J. Geophys. Res.*, *104*(B1), 817–844.

Prieto, G. A., P. M. Shearer, F. L. Vernon, and D. Kilb (2004), Earthquake source scaling and self-similarity estimation from stacking P and S spectra, *J. Geophys. Res.*, *109*.

Rice, J. R., and Y. Ben-Zion (1996), Slip complexity in earthquake fault models, *Proc. Natl. Acad. Sci*, *93*, 3811–3818.

Shearer, P., E. Hauksson and G. Lin (2005), Southern California hypocenter relocation with waveform cross-correlation, Part 2: Results using source-specific station terms and cluster analysis, *Bull. Seismol. Soc. Am.*, *95*, 904-915, doi: 10.1785/0120040168.

Shearer, P. M., G. A. Prieto, and E. Hauksson (2006), Comprehensive analysis of earthquake source spectra in southern California, *Journal of Geophysical Research-Solid Earth*, *111*(B6).

Shearer, P. M. (2009), *Introduction to Seismology*, second edition ed., Cambridge University Press.

Vidale, J. E., and P. M. Shearer (2006), A survey of 71 earthquake bursts across southern california: Exploring the role of pore fluid pressure fluctuations and aseismic slip as drivers, *Journal of Geophysical Research-Solid Earth*, *111*(B5).

Wei, S. J., E. Fielding, S. Leprince, A. Sladen, J. P. Avouac, D. Helmberger, E. Hauksson, R. S. Chu, M. Simons, K. Hudnut, T. Herring, and R. Briggs (2012), Superficial simplicity of the 2010 El Mayor-Cucapah earthquake of Baja California in Mexico, *Nature Geoscience*, *4*(9), 615–618.

Yamashita, T. (1999), Pore creation due to fault slip in a fluid-permeated fault zone and its effect on seismicity: Generation mechanism of earthquake swarm, *Pure and Applied Geophysics*, *155*(2-4), 625–647.

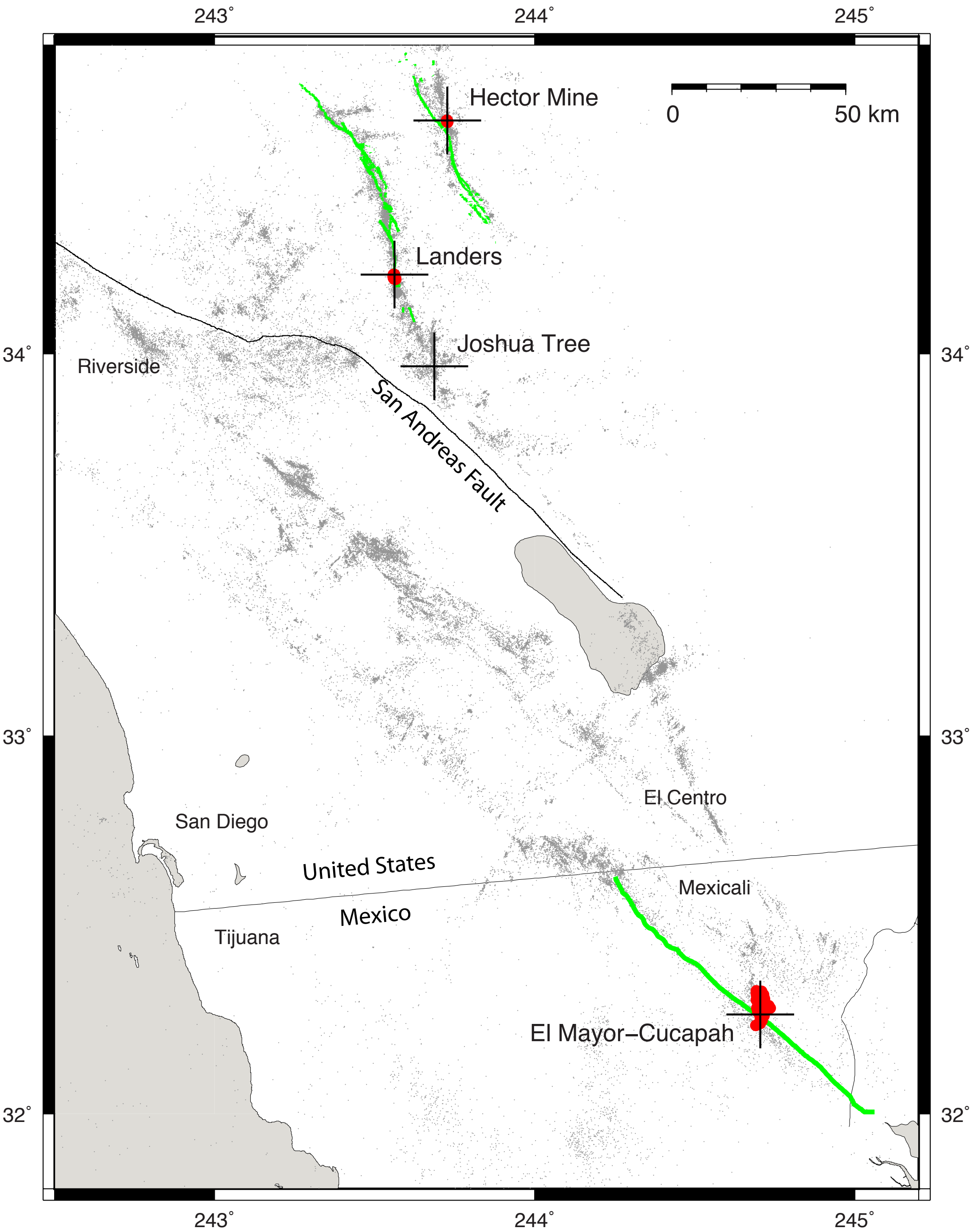

**Figure 1.** A map of southern California, showing the epicenters of three M > 7 mainshocks (black "+"), their foreshocks (red dots) and a random 2% of total seismicity in the region (small grey dots). Green lines are surface fault traces.

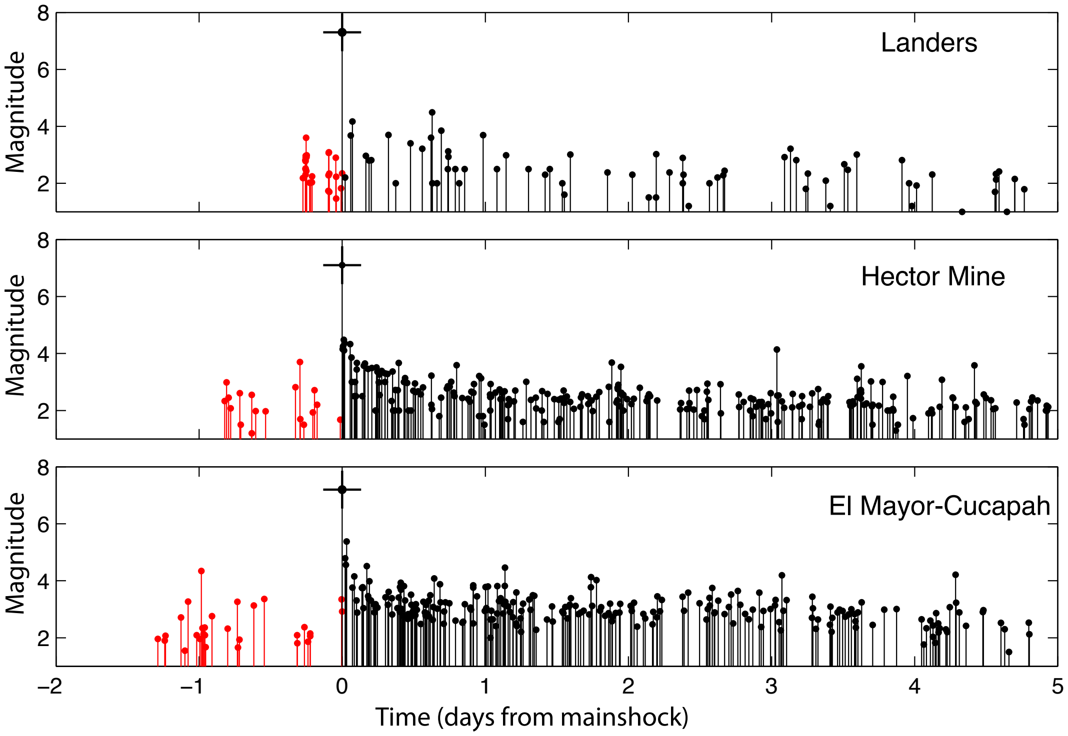

**Figure 2.** Magnitude versus time distributions for the three mainshocks. Forshocks within 3.3 km (6.6 km for El Mayor-Cucapah) and 2 days from mainshocks are shown in red; aftershocks within the same region and 5 days from mainshocks are shown in black.

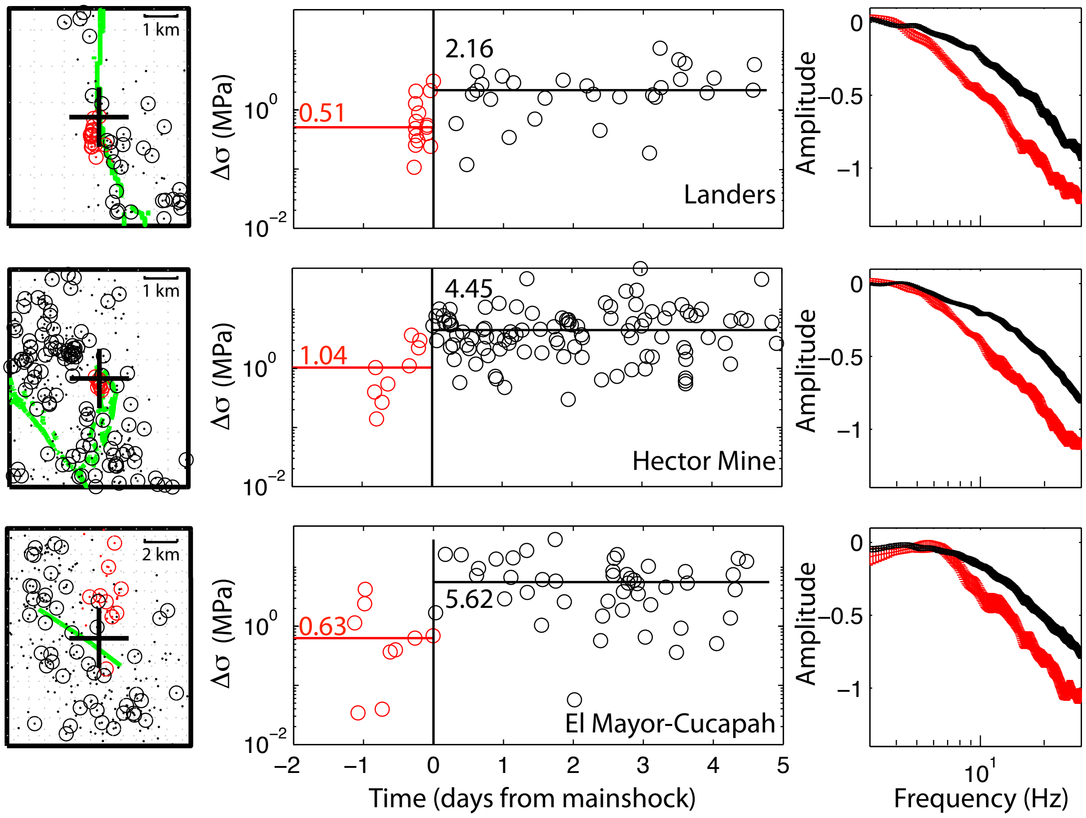

**Figure 3.** Foreshock vs. aftershock comparison. Left column: map view of seismicity, mainshock (shown in black "+") and fault trace (green lines) within the mainshock source region. Middle column: temporal variation of estimated earthquake stress drops (open circles), median values (horizontal lines). Vertical black lines are mainshock occurrence times. Right column: averaged source spectra for foreshocks and aftershocks. In all figures, foreshocks are shown in red, and aftershocks are shown in black. For comparison over a longer time period, see Figures S6 and S7.

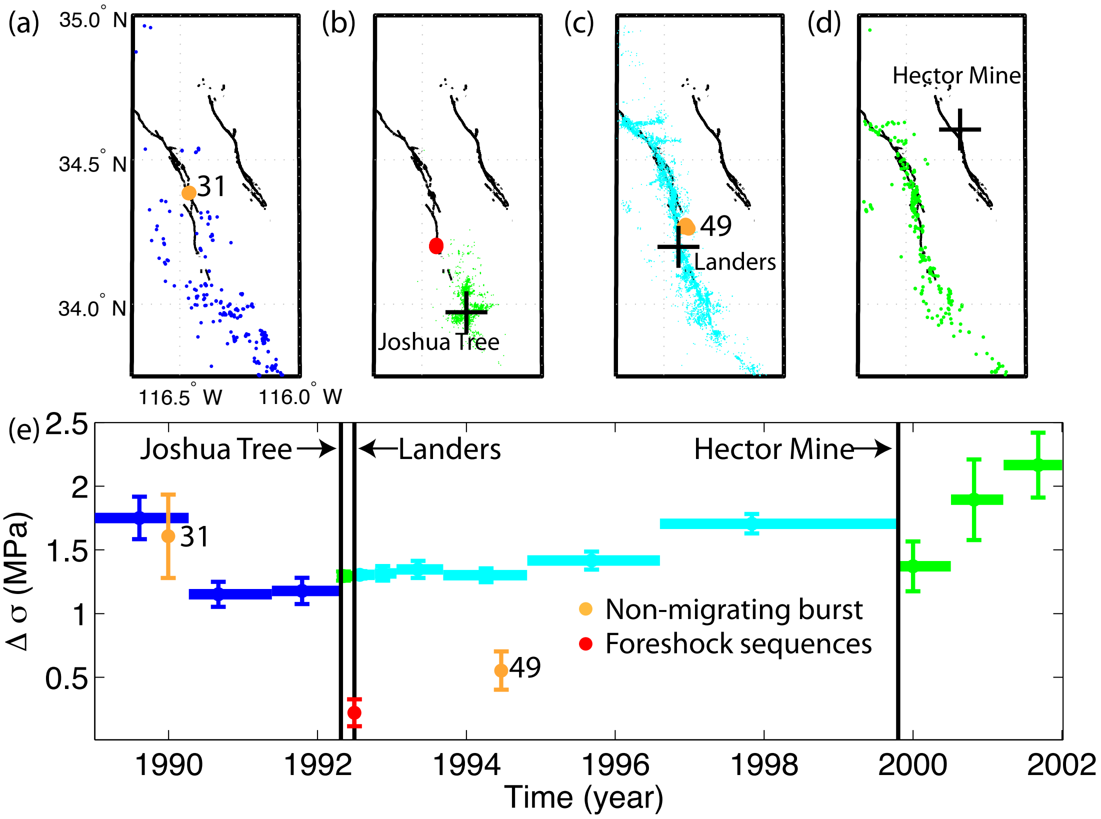

**Figure 4.** Seismicity and stress drops within the Landers fault zone. (a) to (d) Map view of seismicity within different time periods: (a) before the Joshua Tree earthquake; (b) between the Joshua Tree and Landers earthquakes; (c) between the Landers and Hector Mine earthquakes; (d) after the Hector Mine earthquake. The mainshock epicenters are shown in black "+", fault traces are shown in black lines. Foreshock sequences and small seismicity "bursts" (from *Vidale and Shearer* [2006]) are shown in dots with matching colors in (e). (e) Long-term median stress-drop variations within different time periods, with matching colors in (a) to (d), shown in thick horizontal lines. Median stress drops within small clusters are shown in closed circles. Two-standard-error bars are also plotted.

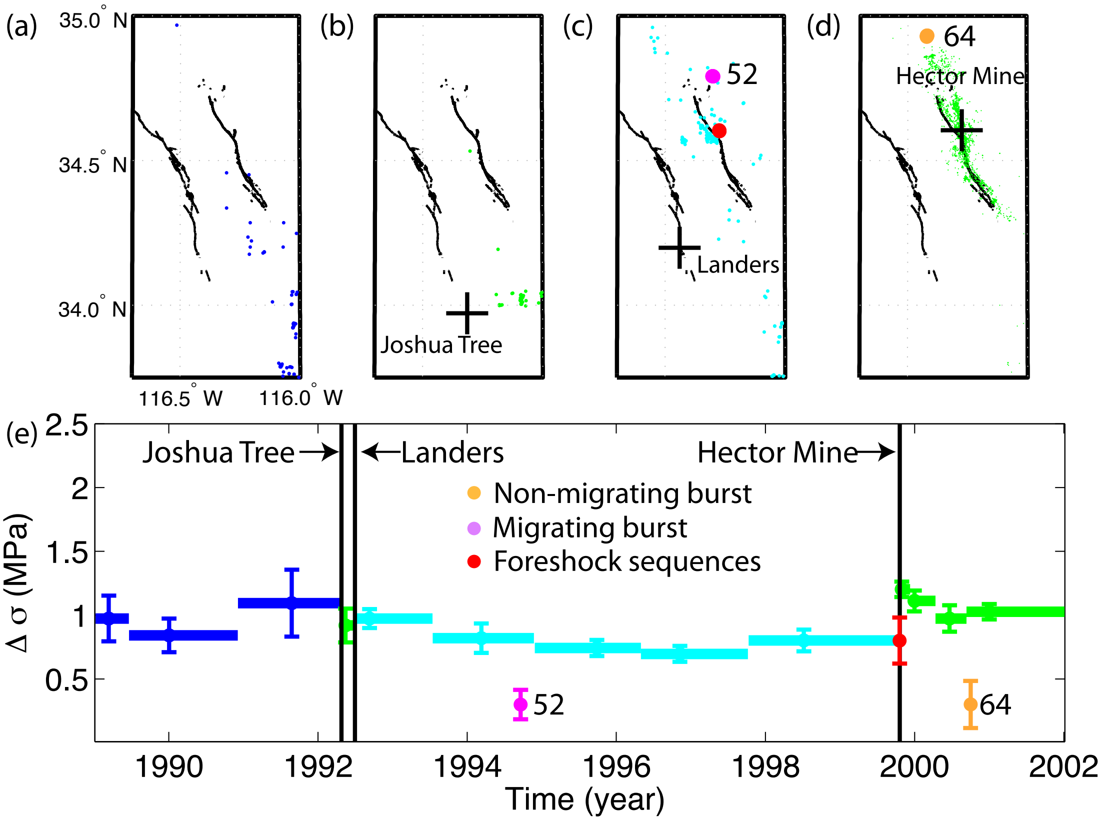

**Figure 5.** Seismicity and stress drops within the Hector Mine fault zone. (a) to (d) Map view of seismicity within different time periods: (a) before the Joshua Tree earthquake; (b) between the Joshua Tree and Landers earthquakes; (c) between the Landers and Hector Mine earthquakes; (d) after the Hector Mine earthquake. The mainshock epicenters are shown in black "+", fault traces are shown in black lines. Foreshock sequences and small seismicity "bursts" (from *Vidale and Shearer* [2006]) are shown in dots with matching colors in (e). (e) Long-term median stress-drop variations within different time periods, with matching colors in (a) to (d), shown in thick horizontal lines. Median stress drops within small clusters are shown in closed circles. Two-standard-error bars are also plotted.